Journal of Physics: Conference Series **1610** (2020) 012001 doi:10.1088/1742-6596/1610/1/012001

Angular zone of influence for fusion and direct reactions on elastic scattering of ^{6}Li with ^{58}Ni, ^{59}Co, ^{64}Ni, and ^{64}Zn

E F Aguilera* **and F Torabi**

Departamento de Aceleradores, Instituto Nacional de Investigaciones Nucleares, Apartado Postal 18-1027, C. P. 11801, México, D. F., México

E-mail: *eli.aguilera@inin.gob.mx

Abstract. Recently, a systematic study of fusion and elastic scattering data was performed for the ^{6}Li + (^{58}Ni, ^{59}Co, ^{64}Ni, ^{64}Zn) systems. Appropriate polarization potentials satisfying the dispersion relation were extracted, which can be associated to fusion and direct reaction couplings, respectively. By examining the relative strengths of the corresponding absorptive parts, a semiclassical analysis can be carried out which gives an indication about the angular range where direct (fusion) reactions are more important in determining the elastic scattering angular distributions. The results of such an analysis are presented for all four systems. The developed method is useful to explore the sensitivity of the elastic scattering angular distributions to the radial details of the phenomenological optical model potential. An example is presented where large sensitivity to distances smaller than the Coulomb barrier radius is evident.

1. Introduction

The study of reactions with loosely bound nuclei, stable or radioactive, has attracted much interest within the nuclear physics community [1, 2]. If one considers only the stable weakly bound nuclei, the most studied one is perhaps ^{6}Li, which in addition maintains a strong current interest [3–15]. The main aim of the present work is to have an in depth sight into the elastic scattering angular distributions measured for ^{6}Li projectiles incident on the particular medium mass targets ^{58}Ni, ^{59}Co, ^{64}Ni, and ^{64}Zn.

It is well known that, in general, elastic scattering angular distributions behave like Rutherford scattering at forward angles and the respective ratio $d\sigma/d\sigma_R$ starts decreasing from 1.0 with increasing angles first because of absorption into direct channels and then also because of absorption into fusion channels. One may wonder whether an angular zone can be identified where the influence of direct reactions predominates and another zone where fusion dominates. If so, is it possible to establish quantitatively a limit between these two angular zones? These questions are addressed here for the four systems mentioned above, taking advantage of the fact that convenient optical model potentials are available for them. Indeed, for the ^{6}Li + (^{58}Ni, ^{59}Co, ^{64}Ni, ^{64}Zn) systems, appropriate polarization potentials satisfying the dispersion relation were recently extracted [15], which can be associated to fusion and direct reaction couplings, respectively. To better illustrate the method, which is introduced here for the first time, the case of the ^{6}Li + ^{64}Zn system will be initially presented. For this particular system, good quality

data exist for elastic scattering [16] which nicely span the energy region near and above the Coulomb barrier, which is the region where the present method can be applied.

Identifying angular zones of influence for particular reaction mechanisms has proved important within different scenarios. In the context of transfer reactions, for instance, it is of fundamental importance to be able to recognize the angular zone where the influence of peripheral reactions is dominant. This is necessary to ensure a reliable extraction of the relevant asymptotic normalization coefficients (ANC's) out from the experimental angular distributions [17, 18]. ANC's regulate the strength of the overlap wavefunction tail. In addition to being of utmost importance in nuclear astrophysics [17], this subject has been shown to play an essential role in the investigation of the short range physics of halo nuclei [19–21]. Considerable effort has been thus dedicated to precisely identify the angular range of data that corresponds to strictly peripheral reactions (see Ref. [21], for instance), with the conclusion that data at low energies and forward angles are most sensitive.

In the context of elastic scattering of heavy ions, on the other hand, the importance of assessing the radial sensitivity of the respective phenomenological optical model potentials has been long recognized [22–24]. Once the sensitive radial region is identified, a quantitative mapping of interaction radius to scattering angle allows one to spot the angular zone of data to which the potential is most sensitive. Although it is generally believed that elastic scattering is able to probe only the nuclear surface [24], within the so called Extended Optical Model (EOM) [25, 26] closer distances can be probed insofar as fusion is additionally reproduced. This model, which has been successfully applied to a large variety of systems, introduces a volume imaginary potential describing absorption under the barrier in addition to the bare and the surface potentials (see Sect. 2). Very recently, it was claimed for several systems that the radial sensitivity function does actually show two peaks, an inner and an outer one [27]. In the case of the imaginary potential, the origin of these peaks was qualitatively identified with fusion and direct reactions, respectively, which further supports the assumptions of the EOM. A novel method based on the phenomenological optical model potentials obtained within the EOM, is introduced in the present work to identify, in the elastic scattering angular distributions, angular zones of dominance for inclusive direct reactions and for fusion.

The present work actually stems from some results recently published by the authors [15], so a summary will be given of such results in Sect. 2. They refer to a systematic analysis of elastic scattering and fusion data of four systems having ^{6}Li projectiles and medium mass targets, where the main questions addressed were: a).- to have a selfconsistent description of fusion and elastic scattering data, and b).- to verify consistency with the Dispersion Relation and/or with either the so called Threshold Anomaly (TA) [28, 29], referring to tightly bound projectiles, or the so called Breakup Threshold Anomaly (BTA) [30, 31], referring to weakly bound stable or radioactive nuclei. In Sect. 3 the present semiclassical method is introduced, illustrating the case of ^{6}Li + ^{64}Zn. The consistency of such semiclassical method with the actual quantum mechanical calculations is analyzed in Sect. 4. In Sect. 5, corresponding zones of influence are obtained for ^{6}Li + (^{58}Ni, ^{59}Co, ^{64}Ni) and, finally, the conclusions are given in Sect. 6.

2. Summary of previous results

The systems analyzed in Ref. [15] are summarized in Table 1. Both fusion and elastic scattering cross sections at near barrier energies have been measured for all these systems, as indicated in the table. The energy range of the respective data is shown and, as a reference, the barrier height is also given in the table. It can be seen that the experimental energy range includes the barrier energy for all data sets.

The respective analysis was performed within the framework of the Extended Optical Model (EOM) introduced by Udagawa and Tamura in the 1980's [25, 26], where the total potential is given by several terms:

Table 1. Data analyzed within the Extended Optical Model in Ref. [15]. The barrier height V_b was obtained in [15] from the Sao Paulo Potential (SPP) [32]

System	measurement	Ref.	$E_{c.m.}(MeV)$	V_b (MeV)
^{6}Li + ^{58}Ni	elastic sc.	[33]	9.0 - 12.7	12.36
	fusion	[3]	9.1 - 12.7	
^{6}Li + ^{59}Co	elastic sc.	[34]	10.9 - 27.2	11.84
	fusion	[35]	10.7 - 23.5	
^{6}Li + ^{64}Ni	elastic sc.	[36]	11.9 - 23.8	12.11
	fusion	[37]	10.5 - 25.6	
^{6}Li + ^{64}Zn	elastic sc.	[16]	10.8 - 20.0	13.05
	fusion	[38]	9.1 - 28.3	

$$U_{TOT} = V_{bare} + V_{Coul} - [iW_{int} + U_F + U_D]. \quad (1)$$

The bare potential, V_{bare}, was taken as the Sao Paulo Potential (SPP) [32], which has no fitting parameters, and for the Coulomb potential V_{Coul}, a radius of 1.2 fm was used; W_{int} is a volume Woods-Saxon potential interior to the barrier, with depth, radius and diffuseness of 50 MeV, 1.0 fm and 0.2 fm, respectively. U_F ($V_F + iW_F$) and U_D ($V_D + iW_D$) are complex polarization potentials that can be associated to fusion and direct couplings, respectively.

The fusion cross section is taken as given by the absorption in both the internal and the fusion polarization potentials ($W_{int} + W_F$). For V_F and W_F a volume Woods-Saxon form was used with common radius and diffuseness ($r_F = 1.4$ fm, $a_F = 0.43$ fm). The respective strengths (V_{F0}, W_{F0}) were taken as fitting parameters. The direct polarization potentials were surface potentials, taken as derivative Woods-Saxon form, whose strengths (V_{D0}, W_{D0}) were fitting parameters. Both the real and the imaginary parts of U_D were supposed to have common values of radius and diffuseness, independent of energy. These values were determined, for each system, from the respective elastic scattering angular distributions by doing a transformation from angle to distance of closest approach on a Rutherford trajectory (see Ref. [15] and also formula 2 below). For the case of the ^{6}Li + (^{58}Ni, ^{59}Co, ^{64}Ni, ^{64}Zn) systems, the values of (r_D, a_D) were (1.61, 0.68), (1.57, 0.84), (1.57, 0.91), and (1.60, 0.85) fm, respectively.

The values of the four free parameters, the strengths of the real and imaginary polarization potentials, were obtained for each individual energy and system by doing a simultaneous fit to the respective elastic scattering angular distribution and corresponding fusion cross section. Along this process, the validity of the dispersion relation was always checked. Good general consistency was found of this relation with the points extracted from the optimization, although there were a couple of exceptions in the fusion polarization potentials for two systems, ^{6}Li + ^{58}Ni and ^{6}Li + ^{64}Zn. The two lowest energy points for these systems showed highly anomalous strength values which did not originally satisfy the dispersion relation, so they were forced to do so. As a consequence, the respective fusion cross sections were underpredicted. However, there are good reasons to believe that the above procedure is correct (see details in Ref. [15]). With these exceptions, very good descriptions were obtained for all reported data about elastic scattering angular distributions, total reaction and fusion cross sections. A conclusion was that the direct polarization potentials obtained for all four systems are consistent with the Breakup Threshold Anomaly, while the respective fusion polarization potentials all follow the Threshold Anomaly rather than the BTA. It is worth noticing that possible uncertainties related to the exceptions mentioned above for ^{58}Ni and ^{64}Zn are not relevant here because they refer to sub-barrier energies. As shall be seen, the present method can be applied only to energies above the

Table 2. Direct and Fusion polarization potentials obtained in Ref. [15] for the ^{6}Li + ^{64}Zn system at $E_{c.m.}$ = 18.1 MeV.

pol. pot.	real str. (MeV)	imag. str. (MeV)	common radius (fm)	common difussenes (fm)
Direct	-0.23	0.28	1.6	0.85
Fusion	5.3	6.0	1.4	0.43

barrier.

3. Method to determine Angular zones of influence. The case ^{6}Li + ^{64}Zn.

The important point most relevant to the present work is that the derived potentials described above nicely fit within the systematics of many data for four different systems, measured at many different energies and angles. It is worth mentioning that the condition of dispersive potentials effectively discarded possible ambiguities in the obtained potentials. In other words, one can say that, within the extended optical model, quite reliable potentials were obtained for the systems of Table 1, in particular for the ^{6}Li + ^{64}Zn system that will be analyzed in the present section. The potential obtained for this latter system at $E_{c.m.}$ = 18.1 MeV, with parameter values given in Table 2, is illustrated in Fig. 1.

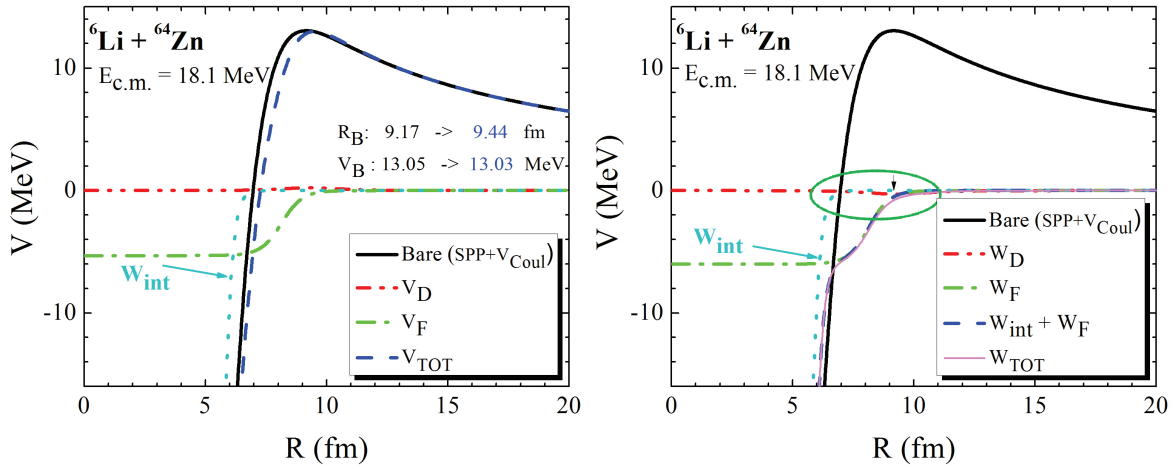

Figure 1. Real (left) and imaginary (right) potentials obtained in Ref. [15] for the ^{6}Li + ^{64}Zn system at $E_{c.m.}$ = 18.1 MeV. For reference, the interior imaginary potential as well as the bare (plus Coulomb) real potential are displayed in both cases. The small arrow indicates the barrier radius. The region of the ellipse is magnified in Fig. 2.

It can be seen that the net effect of the real polarization potentials is a +0.27 fm shift of the barrier radius, keeping essentially the same barrier height. As for the imaginary parts, we are interested in the interplay between the direct and the fusion polarization potentials for radii near the nuclear surface, so an enlargement of the region indicated with the ellipse in Fig. 1 is given in Fig. 2.

At the radius R_T the direct polarization potential and the fusion polarization potential have the same value, so, particles interacting at that distance will feel similar influence from direct

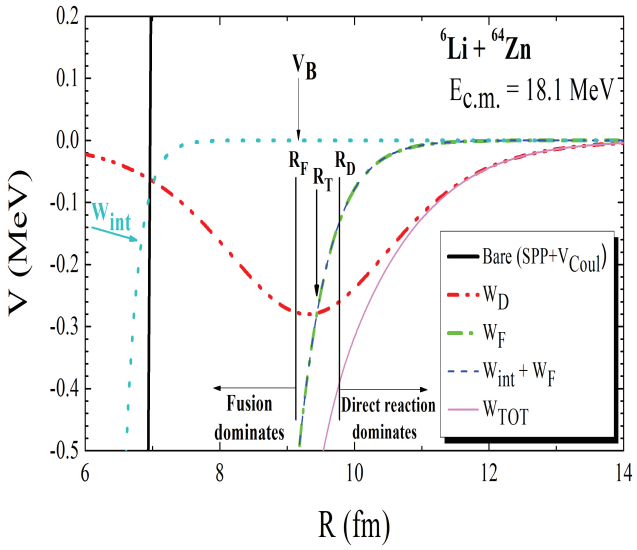

Figure 2. Enlargement of the region indicated with the ellipse in Fig. 1.

and from fusion reactions. At the radius R_D, on the other hand, the strength of the direct part is twice that of the fusion part. All particles interacting at larger distances than R_D will then have a predominant influence from direct reactions. Similarly, particles interacting at smaller distances than R_F (where the strength of the direct part is half that of the fusion part) will feel a predominant influence from fusion. Semiclassically, one can map distance into scattering angle by using the following expressions.

$$D = d(A_p^{1/3} + A_t^{1/3}) = \frac{1}{2} D_0 \left(1 + \frac{1}{sin(\theta_{c.m.}/2)}\right), \quad with\ D_0 = \frac{Z_p Z_t e^2}{E_{c.m.}}, \tag{2}$$

being D the distance of closest approach on a Rutherford trajectory.

The results of such a mapping are illustrated in Fig. 3, where the magenta circles, labeled R_D and R_F, define the limits for the regions of direct-reaction and fusion predominance, respectively. For a given angular distribution, all points above the top magenta circle are in the zone of direct-reaction predominance. Then there is a transition zone, between the two magenta circles, where the influences of direct-reaction and fusion are comparable. Finally, points below the bottom magenta circles correspond to the angular zone where absorption from fusion predominates.

Clearly, the width of the angular zone of influence for direct reactions (fusion) increases (decreases) for lower energies. The angle image of R_D (R_F) corresponds to a nearly constant value of 0.4 (0.25) for the ratio $d\sigma/d\sigma_R$. It would be interesting to find out whether this remains valid for other systems. The semiclassical approach can be applied only for the largest energies in these data sets, because the necessary distance of approach cannot be reached semiclassically for the lowest energies. Naively, one would expect a negligible influence of fusion on the elastic scattering angular distributions corresponding to energies below the barrier. Indeed, it can be shown that using a purely direct polarization potential (i.e., $U_F = 0$) for any of the four systems analyzed in Ref. [15] can yield good fits to the angular distributions corresponding to $E_{c.m.} < V_b$ (but not for $E_{c.m.} \geq V_b$).

4. Consistency with quantum mechanical calculations

In order to investigate the consistency of the present results with the actual quantum mechanical calculations, the effects of including the different terms of the potential in equation 1 are

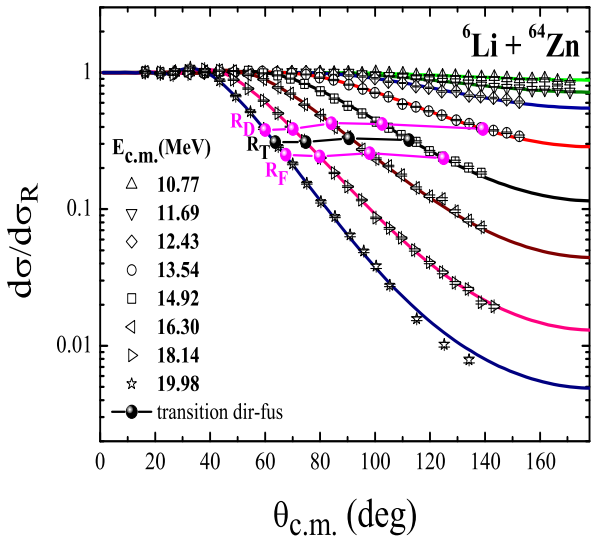

Figure 3. Elastic scattering angular distributions for ^{6}Li + ^{64}Zn. The experimental points are from Ref. [16] while the curves are EOM predictions obtained in Ref. [15]. The angle image of R_D, R_T, R_F was obtained for each energy by replacing D in eq. 2 for the respective value.

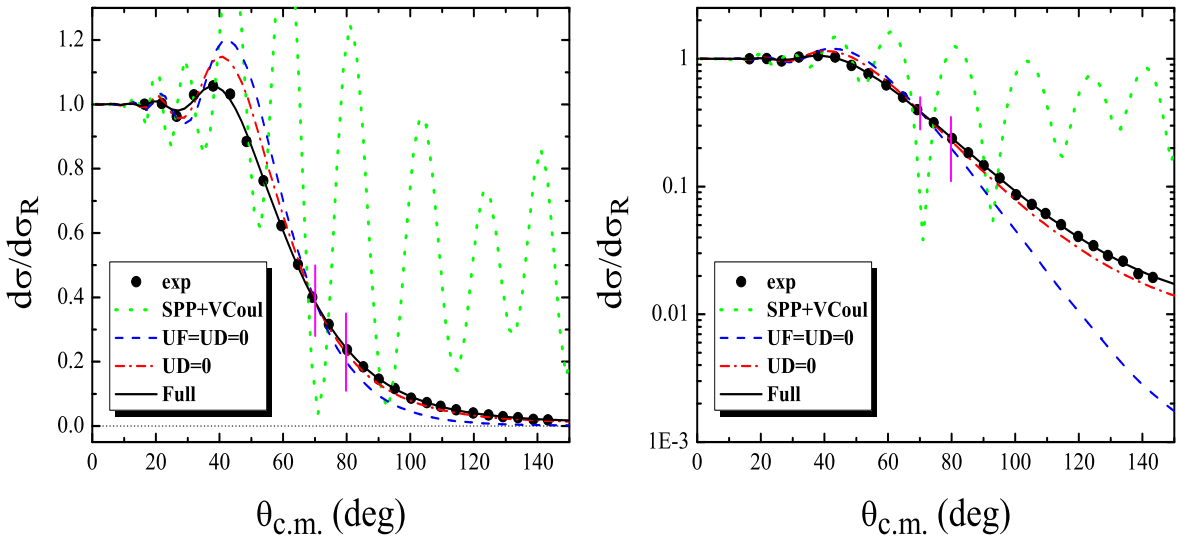

Figure 4. Elastic scattering angular distribution for ^{6}Li + ^{64}Zn at $E_{c.m.}$ = 18.1 MeV . Left: linear scale; right: log scale. The curves are explained in the text.

illustrated in Fig. 4, which corresponds to the case of a center of mass energy of 18.1 MeV for the ^{6}Li + ^{64}Zn system. The green dotted curve was obtained for the case of using only the bare and the Coulomb potentials, switching off both the interior imaginary potential as well as all the polarization potentials. The absence of any absorption in this case leads to reflected waves and the observed oscillations correspond to the superposition of incident and reflected waves. It's interesting to see now what happens when the interior imaginary potential is switched on.

Switching W_{int} on leads to the dashed blue curve; there are no oscillations anymore, so one

can see that the interior imaginary potential has the important role of suppressing the unrealistic reflected waves. This potential provides a condition equivalent to an incoming wave boundary condition, so the flux absorbed in it at this stage would yield the fusion cross section predicted by the one-dimensional barrier penetration model. However, the data are not well described yet: the angular distribution at large angles is underpredicted while at medium angles it is overpredicted. One can see next what is the effect of switching the fusion polarization potential on, which was done in obtaining the red dash-dot curve.

The two violet vertical lines in the figure indicate the mentioned limits for the zones of direct and fusion predominance. It can be seen that the fusion polarization potential is indeed correcting the angular distribution in the region predicted for fusion predominance ($\theta_{c.m.} \geq 79.8$ deg). The difference between the blue dash and the red dash-dot curves reflects the sensitivity of the data to the details of the potential at distances smaller than R_F, which are usually deeper than the nuclear surface (as illustrated in Fig. 2, in the present case the value of R_F, 9.1 fm, is even slightly smaller than the barrier radius, 9.2 fm). The magnitude of such sensitivity can be better appreciated in the log plot at the right hand side of Fig. 4.

On the other hand, the region predicted for direct-reaction predominance, below $\theta_{c.m.} = 70$ deg, is still not well described by the calculation so far. Finally, the additional inclusion of the direct polarization potential (black solid line) leads to a good description also in the region predicted for direct reaction predominance. One can conclude then that the dominance regions predicted within the semiclassical approach are actually consistent with the corresponding quantum mechanical calculations.

5. Angular zones of influence for ^{6}Li + (^{58}Ni, ^{59}Co, ^{64}Ni)

The technique described above to determine corresponding angular zones of influence for ^{6}Li + ^{64}Zn can be easily applied to the other systems analyzed in Ref. [15], i.e., ^{6}Li + (^{58}Ni, ^{59}Co, ^{64}Ni). As mentioned in Sect. 2, proper phenomenological potentials also were obtained for all these systems within the EOM. The corresponding results of the present technique, equivalent to those of Fig. 3, are shown in Fig. 5.

For ^{6}Li + ^{58}Ni, only one energy above the barrier was measured which is so close to the barrier that the corresponding radius R_F cannot be reached semiclassicaly, so only the image angles of R_D, R_T are shown for the respective angular distribution. A similar situation is also valid for the second lowest energy measured for ^{6}Li + ^{64}Ni. For both ^{6}Li + ^{59}Co and ^{6}Li + ^{64}Ni, dominance regions are well defined in the respective data for the three highest-energy angular distributions that were measured.

Interestingly, for all systems in Fig. 5 the angle image of R_D or R_F for the different energies measured also corresponds to nearly constant values of the ratio $d\sigma/d\sigma_R$, as was observed earlier for ^{6}Li + ^{64}Zn. Although the actual values showed a slight variation for the different systems, they were rather similar to each other. For ^{59}Co and ^{64}Ni, the average value of such ratio at (R_D, R_F) was (0.35, 0.24) and (0.41, 0.28), respectively, while for ^{58}Ni the single value obtained for $d\sigma/d\sigma_R$ at R_D was 0.49.

6. Conclusions

A systematic study of four systems performed within the extended Optical Model in Ref. [15], led to reliable potentials satisfying the Dispersion Relation. Taking the corresponding fusion and direct polarization potentials for a given system, a novel method was developed using semiclassical arguments, showing that appropriate angular zones of influence for the respective reaction mechanisms can be defined. Such zones were obtained quantitatively first for the case of the ^{6}Li + ^{64}Zn system, and the corresponding energy dependence was discussed.

While the angular zone of influence for direct reactions becomes wider with decreasing energy, that corresponding to fusion dominance becomes narrower and actually disappears, within the

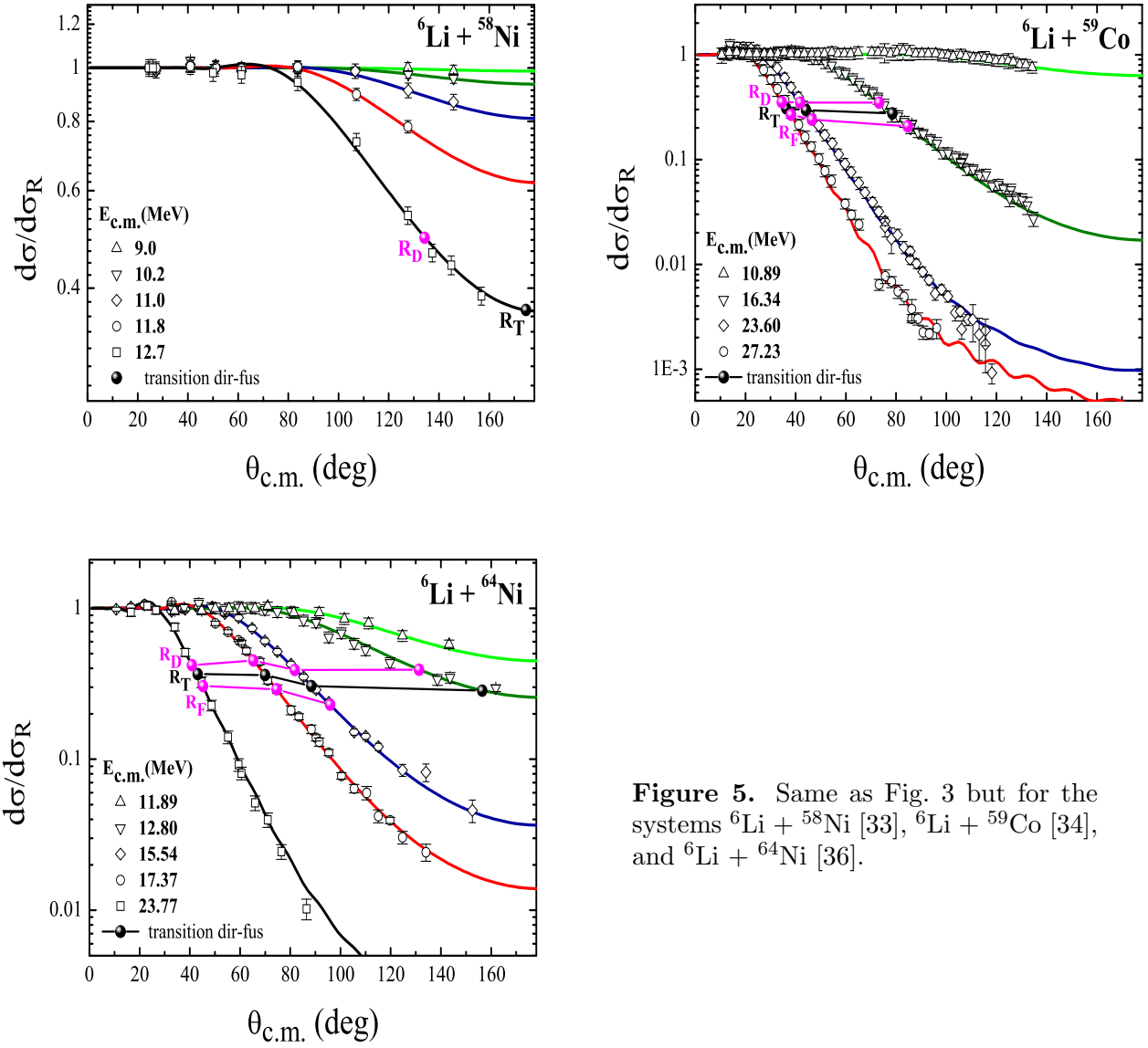

Figure 5. Same as Fig. 3 but for the systems ^{6}Li + ^{58}Ni [33], ^{6}Li + ^{59}Co [34], and ^{6}Li + ^{64}Ni [36].

semiclassical approach, for energies below the barrier. A qualitative consistency with quantum mechanical calculations also was shown. As an important byproduct, the present method clearly shows that distances smaller than the Coulomb barrier radius can be actually probed by elastic scattering measurements. This is consistent with the inner peak observed in the radial sensitivity function in Ref. [27], which was around the barrier radius. Finally, corresponding zones of influence were also obtained for the ^{6}Li + (^{58}Ni, ^{59}Co, ^{64}Ni) systems.

For each analyzed system, independently of the particular energy, the angular zone of predominance for direct reactions roughly corresponded to ratios $d\sigma/d\sigma_R$ larger than some constant value r_D, while that of fusion predominance (not reached by the ^{58}Ni data) could be roughly characterized by values of this ratio lower than some other constant value r_F. These quantities were similar for all systems, with respective mean and standard deviation given by $\langle r_D \rangle = 0.41 \pm 0.06$, $\langle r_F \rangle = 0.25 \pm 0.01$.

Acknowledgments
This work has been partially supported by CONACYT (México) under grant No. CB-01-254619.

References
[1] Canto L F, Gomes P R S, Donangelo R, Lubian J, Hussein M S 2015 *Phys. Rep.* **596** 1
[2] Kolata J J, Guimarães V and Aguilera E F 2016 *Eur. Phys. J.* A **52** 123
[3] Aguilera E F, Martinez-Quiroz E, Amador-Valenzuela P, Lizcano D, García-Flores A, Kolata J J, Roberts A, Rogachev G V, Peaslee G F, Guimarães V, Becchetti F D, Villano A, Ojaruega M, Chen Y, Jiang H, Febbraro M, DeYoung P A, and Belyaeva T L 2017 *Phys. Rev.* C **96** 024616
[4] Zhang G L, Zhang G X, Hu S P, Yao Y J, Xiang J B, Zhang H Q, Lubian J, Ferreira J L, Paes B, Cardozo E N, Sun H B, Valiente-Dobon J J, Testov D, Goasduff A, John P R, Siciliano M, Galtarossa F, Francesco R, Mengoni D, Bazzacco D, Li E T, Hao X, Qu W W 2018 *Phys. Rev.* C **97** 014611
[5] Mukeru B, Rampho G J and Lekala M L 2018 *J. Phys.* G: Nucl. Part. Phys. **45**, 045101
[6] Mukeru B, Rampho G J and Lekala M L 2018 *Nucl. Phys.* A **969** 60
[7] Kabyshev A M, Kuterbekov K A, Sobolev Yu G, Penionzhkevich Yu E, Kubenova M M, Azhibekov A K, Mukhambetzhan A M, Lukyanov S M, Maslov V A, Kabdrakhimova G D 2018 *J. Phys.* G: Nucl. Part. Phys. **45** 025103
[8] Diaz-Torres A, Quraishi D 2018 *Phys. Rev.* C **97** 024611
[9] Aguilera E F, Torabi F 2018 *J. Phys.: Conf. Series* **1078** 012001
[10] Gomez-Camacho A, Wang B, Zhang H Q 2018 *Phys. Rev.* C **97** 054610
[11] Pal A, Santra S, Chattopadhyay D, Kundu A, Jhingan A, Sugathan P, Nayak B K, Saxena A, Kailas S 2019 *Phys. Rev.* C **99** 024620
[12] Lei J, Moro A M 2019 *Phys. Rev. Lett.* **122** 042503
[13] Lei J, Moro A M 2019 *Phys. Rev. Lett.* **123** 232501
[14] Gomez-Camacho A, Diaz-Torres A, Zhang H Q 2019 *Phys. Rev.* C **99** 054615
[15] Torabi F, Aguilera E F, Ghodsi O N, Gomez-Camacho A 2020 *Nucl. Phys.* A **994** 121661
[16] Zadro M, Figuera P, Di Pietro A, Amorini F, Fisichella M, Goryunov O, Lattuada M, Maiolino C, Musumarra A, Ostashko V, Papa M, Pellegriti M G, Scuderi V, and Torresi D 2009 *Phys. Rev.* C **80** 064610
[17] Thompson I J and Nunes F M 2009 *Nuclear Reactions for Astrophysics*, [New York, Cambridge University Press] (www.cambridge.org/9780521856355)
[18] Schröder W U Ed. 2017 *Nuclear Particle Correlations and Cluster Physics*, [Singapore, World Scientific]
[19] Capel P, Phillips D R, Hammer H W 2018 *Phys. Rev.* C **98** 034610
[20] Yang J and Capel P 2018 *Phys. Rev. C* **98** 054602
[21] Moschini L, Yang J, Capel P 2019 *Phys. Rev.* C **100** 044615
[22] Satchler G R 1974 *Proceedings of the International Conference on Reactions between Complex Nuclei, Nashville, Tennessee*, ed B L Robinson, F K McGowan *et al* [New York, North-Holland Amsterdam/American Elsevier] p 171
[23] Moffa P J, Dover C B, and Vary J P 1976 *Phys. Rev.* C **13** 147
[24] Cramer J G, DeVries R M 1980 *Phys. Rev.* C **22** 91
[25] Udagawa T and Tamura T 1984 *Phys. Rev.* C **29** 1922
[26] Udagawa T, Kim B T, and Tamura T 1985 *Phys. Rev.* C **32** 124
[27] Yang L, Lin C J, Jia H M, Wang D X, Ma N R, Wen P W, Yang F, Zhong F P, Zhong S H, and Luo T P 2020 *Phys. Rev.* C **101** 054603
[28] Nagarajan M A, Mahaux C C, Satchler G R 1985 *Phys. Rev. Lett.* **54** 1136
[29] Mahaux C C, Ngô H, Satchler G R 1986 *Nucl. Phys.* A **449** 354
[30] Gomes P R S, Padron I, Fernández Niello J O, Martí G V, Rodríguez M D, Capurro O A, Pacheco A J, Testoni J E, Arazi A, Lubian J, Anjos R M, Chamon L C, Crema E and Hussein M S, 2005 *J. Phys.* G **31** S1669
[31] Hussein M S, Gomes P R S, Lubian J, and Chamon L C 2006 *Phys. Rev.* C **73** 044610
[32] Chamon L C, Carlson B V, Gasques L R, Pereira D, De Conti C, Alvarez M A G, Hussein M S, Cândido Ribeiro M A, Rossi Jr. E S and Silva C P 2002 *Phys. Rev.* C **66** 014610
[33] Aguilera E F, Martinez-Quiroz E, Lizcano D, Gómez-Camacho A, Kolata J J, Lamm L O, Guimarães V, Lichtenthäler R, Camargo O, Becchetti F D, Jiang H, DeYoung P A, Mears P J, and Belyaeva T L 2009 *Phys. Rev.* C **79** 021601(R)
[34] Souza F A, Leal L A S, Carlin N, Munhoz M G, Liguori Neto R, de Moura M M, Suaide A A P, Szanto E M, Szanto de Toledo A, and Takahashi J 2007 *Phys. Rev.* C **75** 044601; C. Beck, *et al*, arXiv:nucl-ex/0411002
[35] Beck C, Souza F A, Rowley N, Sanders S J, Aissaoui N, Alonso E E, Bednarczyk P, Carlin N, Courtin S, Diaz-Torres A, Dummer A, Haas F, Hachem A, Hagino K, Hoellinger F, Janssens R V F, Kintz N, Liguori

Neto R, Martin E, Moura M M, Munhoz M G, Papka P, Rousseau M, Sànchez i Zafra A, Stézowski O, Suaide A A, Szanto E M, Szanto de Toledo A, Szilner S, and Takahashi J 2003 *Phys. Rev.* C **67** 054602

[36] Biswas M, Subinit Roy, Sinha M, Pradhan M K, Mukherjee A, Basu P, Majumdar H, Ramachandran K, Shrivastava 2008 *Nucl. Phys.* A **802** 67

[37] Moin Shaikh Md, Subinit Roy, Rajbanshi S, Pradhan M K, Mukherjee A, Basu P, Pal S, Nanal V, Pillay R G, and Shrivastava A 2014 *Phys. Rev.* C **90** 024615

[38] Di Pietro A, Figuera P, Strano E, Fisichella M, Goryunov O, Lattuada M, Maiolino C, Marchetta C, Milin M, Musumarra A, Ostashko V, Pellegriti M G, Privitera V, Randisi G, Romano L, Santonocito D, Scuderi V, Torresi D, and Zadro M 2013 *Phys. Rev.* C **87** 064614